Short-Range Cut-Off of the Summed-Up van der Waals Series: Rare-Gas Dimers

Abhirup Patra, Bing Xiao, and John P. Perdew

Abstract van der Waals interactions are important in typical van der Waals-bound systems such as noble gas, hydrocarbon, and alkaline earth dimers. The summed-up van der Waals series of Perdew et al. 2012 works well and is asymptotically correct at large separation between two atoms. However, as with the Hamaker 1937 expression, it has a strong singularity at short non-zero separation, where the two atoms touch. In this work we remove that singularity (and most of the short-range contribution) by evaluating the summed-up series at an *effective* distance between the atom centers. Only one fitting parameter is introduced for this short-range cut-off. The parameter in our model is optimized for each system, and a system-averaged value is used to make the final binding energy curves. This method is applied to different noble gas dimers such as Ar–Ar, Kr–Kr, Ar–Kr, Ar–Xe, Kr–Xe, Xe–Xe, Ne–Ne, He–He, and also to the Be_2 dimer. When this correction is added to the binding energy curve from the semilocal density functional *meta*-GGA-MS2, we get a vdW-corrected binding energy curve. These curves are compared with the results of other vdW-corrected methods such as PBE-D2 and vdW-DF2, and found to be typically better. Binding energy curves are in reasonable agreement with those from experiment.

Keywords van der Waals · Density functional · Binding energy curves · Rare-gas dimers · Summation of asymptotic series

A. Patra (✉) and J.P. Perdew
Department of Physics, Temple University, Philadelphia, PA 19122, USA
e-mail: tuf43805@temple.edu; tuf25956@temple.edu

B. Xiao
Department of Earth Sciences, University College London, London WC1E 6BT, UK
e-mail: b.xiao@ucl.ac.uk

Contents

1 Introduction

Theoretical prediction of matter and proper explanation of many physical, chemical, and biological processes require an accurate description of atomic and molecular interactions. The only way to get a clear picture of these interactions at the atomic and molecular level is to apply quantum mechanics. Much effort has been made to develop quantum mechanical methods for this purpose. As a result there are many wave-function-based ab initio quantum mechanical methods such as Configuration Integration (CI), Many Body Perturbation Theory (MBPT), and Quantum Monte Carlo (QMC) which are popular in the scientific community. However, the Kohn–Sham (KS) [1] density functional theory (DFT) [2] has become the most popular in condensed matter physics and in quantum chemistry, because of its low computational cost and reasonable accuracy. It maps a many-electron wave-function problem to a one-electron problem. The many-electron effects are in its exchange-correlation part E_{XC}. This exchange-correlation functional E_{XC} is often approximated through satisfaction of various physical constraints.

Among numerous exchange-correlation approximations, the local spin density approximation (LSDA) [1–4], the Perdew-Burke-Ernzerhof (PBE) [5] generalized gradient approximation (GGA), and the Becke-3-Lee-Yang-Parr (B3LYP) [6] and HSE03 [7, 8] hybrid GGAs are especially popular in DFT [9] calculations for

physical and chemical systems. LSDA and PBE are efficient local and semilocal functionals widely used for extended systems, whereas PBE0 and HSE06 are hybrid functionals which hybridize a GGA with the exact exchange energy. Another hybrid functional B3LYP has a more complicated mixing of LDA and GGA exchange functionals with HF exact exchange, and its correlation energy part is also a mixing of LDA and GGA. These hybrid functionals are popular for calculations in both finite and extended systems. At the semilocal level, however, the *meta*-GGA is the highest rung of the so-called Jacob's ladder of DFT [10, 11] and potentially the most accurate one [12]. *Meta*-GGA can also serve as a better base for hybridizing with the exact exchange energy.

At the semilocal level, the E_{XC} of density functional theory can be written as [3, 4, 12–14]

$$E_{XC}^{sl}[n_\uparrow, n_\downarrow] = \int d^3 r n \epsilon_{XC}^{sl}(n_\uparrow, n_\downarrow, \nabla n_\uparrow, \nabla n_\downarrow, \tau_\uparrow, \tau_\downarrow). \tag{1}$$

In this equation, $n_\uparrow$, $n_\downarrow$ are the electron densities of spin up and down $\sigma_\uparrow$, $\sigma_\downarrow$ respectively, and the $\nabla n_\uparrow$, $\nabla n_\downarrow$ are the local gradients of the spin densities. The kinetic energy densities are $\tau_\sigma = 1/2 \sum_k |\nabla \psi_{k,\sigma}|^2$ for the occupied KS orbitals $\psi_{k\sigma}$ of spin σ, and ϵ_{XC}^{sl} is the approximate exchange-correlation energy per electron. LSDA uses only $n_\uparrow, n_\downarrow$ whereas GGAs use $\nabla n_\uparrow, \nabla n_\downarrow$ in addition. *Meta*-GGAs [15–17] also use the kinetic energy density τ_σ as one of its ingredients. This τ_σ has information about the shell structure. The τ-dependence of *meta*-GGAs has been studied by Sun et al. [18, 19]. *Meta*-GGAs can distinguish different orbital-overlap regions by "α", defined as $\alpha = \frac{\tau - \tau^W}{\tau^{unif}}$ where $\tau = \sum_\sigma \tau_\sigma, \tau^W = \frac{1}{8} |\nabla n|^2 / n$ and $\tau^{unif} = \frac{3}{10}(3\pi^2)^{2/3} n^{5/3}$. Sun et al. [20] showed that different values of α recognize three different typical regions: (1) $\alpha = 0$ in the single-orbital regime with one- and two-electron densities which characterize covalent single bonds, (2) $\alpha \approx 1$ in the slowly-varying density regime that characterizes the metallic bond, and (3) $\alpha \geq 1$ in the weakly-overlapped density region which characterizes a noncovalent bond.

In principle, DFT provides exact ground-state energies and densities, but in practice there are many situations where DFT fails to give a physical result. The long-range van der Waals interaction in rare gas dimers [21, 22], hydrocarbons, and alkaline earth diatomics is one of them. There have been many tests of density functional theory in rare gas dimers and alkaline earth dimers. Tao and Perdew [23] observed that the GGA of Perdew, Burke, and Ernzerhof (PBE) [5], the *meta*-GGA of Tao, Perdew, Staroverov, and Scuseria (TPSS) [11, 12], and its hybrid version (TPSSh) [23] all give a satisfactory and reasonable description of the short-range part of the van der Waals interaction in the van der Waals bound complexes which have strong density overlap. The authors Tao and Perdew [23] concluded that these functionals predict too-long bond lengths and too-small binding energies for the rare gas dimers, which can be improved by long-range correction of the van der Waals interaction. Ruzsinszky et al. [24] have tested non-empirical GGAs and *meta*-GGAs and found that GGAs and *meta*-GGAs tend to overbind the diatomics

with valence "s" electrons such as He_2 and Be_2 while underbinding the diatomics with valence "p" electrons such as Ar_2.

van der Waals interactions [25] are important for many material properties. The source of this weak, long-range interaction between two objects is instantaneous charge fluctuation. The van der Waals interaction is important in atomic and molecular systems, where it has many implications such as heat of sublimation of hydrocarbon molecules, chemical reaction precursor complexes, energy transfer intermediates, protein folding, stacking of nucleobases, crystal packing, and self-assembly of organic molecules. Long-range van der Waals interaction between two distinct objects requires full density-functional non-locality. There are many long-range correction methods [26–29] developed in the last few years which are good for predicting van der Waals (vdW) interaction. These also include many post Hartree–Fock (HF) methods [30–33]; see Klimeš and Michaelides [34] for an overall review of DFT-based dispersion methods. Tao et al. [35] developed a reliable approach to evaluate accurately the dynamic multipole polarizabilities and higher order vdW coefficients from electron densities and static multipole polarizabilities for spherical atoms or objects, without using any empirical fitting parameter.

Perdew et al. [36, 37] have discussed the vdWinteraction. For two spherical objects of radius R separated by a distance d, second-order perturbation theory gives the attractive long-range van der Waals interaction [38]

$$E_{vdW} = -\frac{C_6}{d^6} - \frac{C_8}{d^8} - \frac{C_{10}}{d^{10}} - \dots \tag{2}$$

The above expression is valid for $d \to \infty$. Here C_6 describes the dipole–dipole interaction, C_8 the dipole–quadrupole interaction, and C_{10} the quadrupole–quadrupole interaction and the dipole–octupole interaction. In Ruzsinszky et al. [39] these coefficients are modeled accurately and analytically for classical solid-spheres (nanoclusters) and shells (fullerenes) using the static dipole polarizability.

Furthermore, Perdew et al. [38] proved that the above asymptotic expansion can be summed to all orders for two identical spherical shells. In that work a possible two-parameter solution to the divergence problem in van der Waals interactions at very short atomic separation has also been discussed. Such divergences (which occur at $d = 0$ for any finite-order series but at $d > 0$ for the summed-up infinite series) are normally removed by a damping function [40]. Inspired by Perdew et al. [38], we suggest that a physical summation of the vdW series [35] can be used for long-range correction of semilocal density functionals, which by themselves do not have any long-range vdW interaction correction.

In this chapter we discuss a simplified cut-off approach based on the summed-up asymptotic series. This method uses only one parameter, optimized here for different systems and averaged for all systems, which can usefully provide the long-range part of the van der Waals interaction when added to the calculated binding energy curves from the *meta*-GGA-MS2 [18, 20].

2   Methods

2.1   Asymptotic van der Waals Series

The van der Waals interaction between two spherical-shell objects A and B (with thickness "t", radius "R", and electron density "ρ") can be found from (10) of Perdew et al. [38] as the infinite series

$$E(d) = -\sqrt{4\pi\rho} \sum_{k=3}^{\infty} c_k(t/R) z^k, \qquad (3)$$

where d is the distance between the centers of the two objects, $z = \left(\frac{2R}{d}\right)^2$, and all equations are in atomic units. The reduced coefficient $c_k(t/R)$ is defined by $C_{2k} = c_k(t/R)\sqrt{4\pi\rho}\left[(2R)^2\right]^k$. When the geometric series $\sum_{k=1}^{\infty} z^k = (1-z)^{-1}$ for $0 \le z < 1$ is introduced and the approximation $c_k \to c_\infty$ is used for $k > 5$, we find that (3) can be summed up as [38]

$$E^{\text{geo}}(d) = -\sqrt{4\pi\rho}\left[c_3\left(\frac{t}{R}\right)z^3 + c_4\left(\frac{t}{R}\right)z^4 + c_5\left(\frac{t}{R}\right)z^5 + c_\infty\left\{ (1-z)^{-1} - \sum_{k=0}^{5} z^k \right\}. \qquad (4)$$

(See Appendices 1 and 2 for details; also see Table 1 for the values of $c_k(t/R = 1)$.)

The important message from Table 1 is that the reduced coefficients tend to a constant value as $k \to \infty$. This means that the higher-order terms of (3) can be summed as a geometric series $\sim (1-z)^{-1}$, leading to an analytic closed-form expression which sums up this asymptotic ($d \to \infty$) series. The resulting expression for $E^{\text{geo}}(d)$ (4) approximately sums the asymptotic van der Waals series to all orders in d^{-1}, but diverges at very short atomic separation when the two spheres touch

Table 1 Values of reduced van der Waals coefficients at $t/R = 1$ (solid spheres)

Values of $c_k(t/R = 1)$	
Coefficient	Values for $t/R = 1$
c_3	0.006766 (0.006766)
c_4	0.008842 (0.0101015)
c_5	0.009599 (0.01217)
c_6	0.009946
c_{10}	0.010447
c_{20}	0.010761
c_{40}	0.010904
c_{80}	0.010979
c_∞	0.011 (0.020)

Values from the Hamaker [41] expression are in parentheses. The Hamaker expression has one adjustable parameter, chosen here to make the lowest-order coefficients agree (from Perdew et al. [38])

each other. The corresponding separation is $d = R_A + R_B$ for two non-identical spheres and $d = 2R$ for two identical spheres, but the true van der Waals interaction energy remains finite there. Thus, the summed-up expression must be cut off at small d while remaining unchanged to all orders in d^{-1} at large d. The simplest way to do this is to replace d by d', where the difference between d' and d vanishes exponentially as $d \to \infty$. Perdew et al. [38] suggested a possible choice for d':

$$d' = d + g\exp[-(d - 2R)/h] \tag{5}$$

which ensures $d' > 2R$ for $g > 0$ and $h > 0$. In that work, Perdew et al. [38] have also shown that reasonable parameters for C_{60}–C_{60} are $g = 10$ and $h = 2$ atomic units. These parameters are of course system-dependent. We assume that the summed-up series is only valid when d is sufficiently greater than $2R$. Each choice of $g > 0$ and $h > 0$ defines a different asymptotic summation of (3) to all orders in d^{-1}.

In this work we have chosen instead the simplest possible form:

$$y' = y + a\exp\left(-\frac{y}{a}\right). \tag{6}$$

Here $y' = \frac{d'}{R}$, and $y = \frac{d}{R}$. $a > 2$ is a parameter. It should be noted that y' starts out as $a = \frac{y^2}{2a}$ at small y, then increases monotonically, approaching y exponentially at large y. Moreover, $a > 2$ guarantees that the singularity is removed. (To establish that y' is monotonic in y for non-negative y, just compute $\frac{dy'}{dy} = 1 - \exp\left(-\frac{y}{a}\right) \geq 0$.) We have considered $E(d')$ as an additive correction to the binding energy curve of a semilocal density functional such as GGA or *meta*-GGA. For each functional, we adjust the parameter "a" to obtain the best overall fit to known accurate reference binding energy curves. PBE GGA needs a smaller value of "a", which more significantly shortens the equilibrium bond length and strengthens the binding. The *meta*-GGA Made Simple (MGGA-MS2), which captures more of the intermediate-range vdW interaction, needs a larger value of "a", providing a correction which is less short-ranged and has less effect on the equilibrium bond length and binding energy. It should be noted that the fitting is done only for the range of d greater than or equal to the reference equilibrium bond length, because we cannot expect any useful correction of short-range errors in the functional from this approach. Here we present the vdW-corrected binding energy curves calculated by MGGA-MS2, which should give us a proper insight into the summed-up series expansion of the van der Waals interaction.

2.2 Physical Explanation of R

Let $R = (R_A + R_B)/2$ be the arithmetic average of the radii of the two spherical objects A and B. If the objects are classical metallic spheres with uniform density

inside and zero density outside a cutoff radius, then the radius of a sphere is clearly the only relevant length scale for that sphere. One could find polarizability radii $R_A = \left[\alpha_1^A(0)\right]^{\frac{1}{3}}$ and $R_B = \left[\alpha_1^B(0)\right]^{\frac{1}{3}}$, where $\alpha_1^A(0)$ and $\alpha_1^B(0)$ are the static dipole polarizabilities of A and B, or one could find the same radius R from $R = R^{hbl} =$ half the equilibrium bond length of a dimer, because two such spheres would be attracted to one another right up to the point where they touched. In this case, there is no decay length for the density of a sphere (as in (6)), but the summed-up van der Waals interaction must still be cut off to avoid a spurious divergence to minus infinity when the spheres touch. This shows that R_A is indeed the radius of object A.

This gives us an insight: the infinite van der Waals series (2) is an asymptotic series, valid only when the "aspect ratio" R/d is small enough. This series can be summed to all orders, but that summation misses contributions which are important when the aspect ratio is not small. Only when the objects are so far apart that each "looks small" to the other is the summed-up van der Waals series accurate.

When we extend these ideas from pairs of classical metallic spheres to pairs of atoms, we can no longer expect that $R^{pol} = R^{hbl}$. We need to choose between these two alternatives. Simple density functionals for R are not expected to work because the static polarizability of a classical metallic sphere depends only on the radius, and not on the density inside that sphere (e.g., Perdew et al. [38] and Ruzsinszky et al. [39]). We have found empirically, for rare gas and alkaline earth dimers (Be_2), that we can obtain a reasonable long-range correction to the binding energy curve of MGGA-MS2 [19] using a system-averaged value of the fitting parameter "a" (see Table 2) along with

$$R = \max\left[R^{hbl}, 1.37R^{pol}\right]. \tag{7}$$

This is R^{hbl} for all considered rare gas atoms, but $1.37R^{pol}$ for Be. This choice guarantees that the singularity of the summed-up vdW series is removed for any pair of spherical objects. It should be noted that this R^{hbl} is basically the half-bond length of any homo-dimer (A_2) and hetero-dimer (AB) which can be defined as

$$R_A^{hbl} = R_{AA}/2 \tag{8}$$

for homo- and

Table 2 Optimized values of the fitting parameter "a" for different rare-gas dimers

Optimized values of "a" from MGGA-MS2 + vdW[d']							
Fitting parameter	Ar–Ar	Kr–Kr	Xe–Xe	Ar–Kr	Ar–Xe	Kr–Xe	System-averaged "a".
a	2.19	2.14	2.00	2.00	2.125	2.09	2.09
Optimized values of "a" from MGGA-MS2 + H[d']							
a	2.86	2.52	2.14	2.46	2.45	2.33	2.46

$$R_{AB}^{hbl} = (R_{AA} + R_{BB})/2 \tag{9}$$

for hetero-dimers. We take R_{AA} from the experimental binding energy curve.

3   Computational Details

3.1   Calculation of Dimer Binding Energy

The binding energies of different pairs of atom have been calculated in the projector augmented wave approach (PAW) [42] implemented in the Vienna ab initio simulation package (VASP) [43–45] within *meta* generalized gradient approximation (MGGA-MS2) for the exchange-correlation functional. In the calculations, the kinetic energy cutoff is first set to be 600 eV, and a Γ centered $1 \times 1 \times 1$ k-point mesh in the BZ is used for the k-space integration. The total energy of the atomic pairs has been calculated using a $10 \times 20 \times 10$ rectangular super-cell. The PAW scheme is utilized with the potentials taken from the VASP PBE library. The energy of an isolated atom is calculated by a $10 \times 10 \times 10$ cubic super-cell. The binding energy is calculated in the following way:

$$\Delta E = -[E(R_{dimer}) - 2 \times E(R_{Atom})]. \tag{10}$$

We have also used other van der Waals methods, PBE-D2 [27] and vdW-DF2 [46], to perform this calculation. All these DFT methods are available in VASP. Our long-range-corrected *meta*-GGA-MS2 seems to give better results than these two vdW-corrected functionals.

3.2   Optimization of the Fitting Parameter

The average error (AE) calculation and the additive correction to the DFT results have been made in computer codes. The inputs to these codes are the binding energy curves calculated using DFT ($E_{MGGA-MS2}$), static dipole polarizabilities, and electron densities for each atom of the pair, and van der Waals coefficients C_6, C_8, C_{10}. Reference values for comparison are the experimental binding energy curves [47, 48].

There is a strong singularity near $d = 2R$ in the summed-up van der Waals series, as discussed before. To remove it, we replace y and y' in (6) by d/R and d'/R, respectively, to get

$$d' = d + aR\exp\left[-\frac{d}{aR}\right] \tag{11}$$
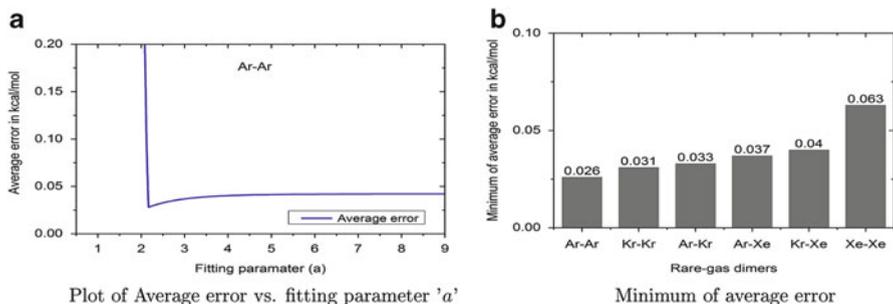
Fig. 1 (**a**) Plot of average error vs fitting parameter "*a*" for Ar–Ar. (**b**) Plot of minimum average error for different rare gas dimers

with R^{hbl} for rare-gas dimers and $R = 1.37R^{\text{pol}}$ for Be_2. This d' is used to calculate the summed-up $E(d')$. In this section, we use $E(d')$ from (14) below as the long-range van der Waals correction to be added to the MGGA-MS2 binding energy curve.

We have optimized the fitting parameter "*a*" by minimizing the error between the binding energy curve from the vdW-corrected method and the experimental binding energy curve over the set of d's in the range $d_{\min} \text{Å} < d < 9 \text{ Å}$ in steps of 0.1 Å for each dimer. Here $d_{\min} \text{Å}$ is the separation at the minimum in the experimental binding energy curve. The fitting parameter "*a*" in (11) is varied in the range $0.0 < a < 10.0$ in steps of 0.001 to maintain accuracy. The average error (AE) at each value of "a" is calculated using

$$\text{AE}\big|_a = \left[\sum_{d'=d_{\min}}^{9} \left| E_{\text{MGGA-MS2+vdW}}\left(d'\right) - E_{\text{Exp}} \right| \right] \Big/ \left(\text{Total number of } d' \text{ points} \right).$$

(12)

Figure 1a shows the average error vs fitting parameter "*a*" plotted for the Ar_2 dimer. Figure 1b shows a histogram plot of minimum average error (MAE) for different rare gas dimers. MAE is the minimum of the average error at the optimized value of "*a*" for each system. So this is a discrete-column graph where each column gives the error at the minimizing value of "*a*".

3.3 Calculation of the van der Waals Interaction Corrected Binding Energy

To avoid the system dependence of the fitting parameter, the system-averaged value of the fitting parameters "*a*" was used to recalculate all the binding energy curves.

We found that the system-averaged fitting parameter gives us even better correction in most cases. In this work, all the binding energy curves are calculated using the system-averaged fitting parameter "a_{sys}" (see Table 2). Replacing "a" with "a_{sys}", (11) becomes

$$d' = d + a_{\text{sys}}R\exp\left(-\frac{d}{a_{\text{sys}}R}\right). \tag{13}$$

Finally, the vdW-corrected energy is calculated by replacing $E(d)$ by $E(d')$. The correction part is calculated using Hamaker's expression $E^{\text{H}}(d)$ as modified in Perdew et al. [38]:

$$E_{\text{vdW}}\left(d'\right) = \left(-\frac{C_6}{d'^6} - \frac{C_8}{d'^8} - \frac{C_{10}}{d'^{10}}\right) + \left(\frac{C_\infty}{C_\infty^{\text{H}}}\right)\left[E^{\text{H}}\left(d'\right) + \frac{C_6^{\text{H}}}{d'^6} + \frac{C_8^{\text{H}}}{d'^8} + \frac{C_{10}^{\text{H}}}{d'^{10}}\right] \tag{14}$$

and then added to the MGGA-MS2 result

$$\begin{aligned}
E_{\text{MGGA-MS2+vdW}}\left(d'\right) &= E_{\text{vdW}}\left(d'\right) + E_{\text{MGGA-MS2}}(d) \\
&= \left(-\frac{C_6}{d'^6} - \frac{C_8}{d'^8} - \frac{C_{10}}{d'^{10}}\right) + \left(\frac{C_\infty}{C_\infty^{\text{H}}}\right)\left[E^{\text{H}}(d') + \frac{C_6^{\text{H}}}{d'^6} + \frac{C_8^{\text{H}}}{d'^8} + \frac{C_{10}^{\text{H}}}{d'^{10}}\right] \\
&\quad + E_{\text{MGGA-MS2}}(d).
\end{aligned} \tag{15}$$

It should be noted that by $E^{\text{H}}(d)$ we mean Hamaker's [41] classical expression for the van der Waals interaction energy $E^{\text{H}}(R_{\text{A}}, R_{\text{B}}, d)$ between two spherical objects of radii R_{A}, and R_{B} when the two centers are separated by a distance "d". This $E^{\text{H}}(R_{\text{A}}, R_{\text{B}}, d)$ is given by the following equation:

$$E^{\text{H}}(R_{\text{A}}, R_{\text{B}}, d) = -\frac{\pi^2\beta}{6}\left\{\frac{2R_{\text{A}}R_{\text{B}}}{d^2 - (R_{\text{A}} + R_{\text{B}})^2} + \frac{2R_{\text{A}}R_{\text{B}}}{d^2 - (R_{\text{A}} - R_{\text{B}})^2} + \ln\left[\frac{d^2 - (R_{\text{A}} + R_{\text{B}})^2}{d^2 - (R_{\text{A}} - R_{\text{B}})^2}\right]\right\} \tag{16}$$

where $\beta = c_3(1)\sqrt{4\pi}\rho\left(\frac{3}{4\pi}\right)^2 2^6 = 0.006766\sqrt{4\pi}\rho\left(\frac{3}{4\pi}\right)^2 2^6$ is evaluated using the value of $c_3(1)$ from Table 1. The electron density is $\rho = \frac{N}{\left(\frac{4}{3}\pi R^3\right)}$ for a sphere with radius R. N is the total number of valence electrons (2 for He and 8 for the other rare gas atoms). For non-identical spheres, we replace $\sqrt{\rho}$ by $2\sqrt{\rho_{\text{A}}}\sqrt{\rho_{\text{B}}}/\left(\sqrt{\rho_{\text{A}}} + \sqrt{\rho_{\text{B}}}\right)$.

The van der Waals coefficients (C_6, C_8, C_{10}) used in the first part of the right-hand side of (15) are taken from their tabulated values in the supporting informa-tion of [35]. All these standard van der Waals coefficients are calculated by time-dependent Hartree-Fock theory. The van der Waals coefficients from

Hamaker's formula (C_6^H, C_8^H, C_{10}^H) in the second part of the right-hand side of the same equation are evaluated by extracting the coefficients of d^{-6}, d^{-8}, and d^{-10} from the Taylor series expansion of the expression of $E^H(R_A, R_B, d)$ of (16) in power of d^{-1}:

$$E^H(R_A = R_B = R, d) = -\frac{\pi^2 \beta}{6} \left(\frac{32 R_A^3 R_B^3}{3d^6} + \frac{32 R_A^3 R_B^3 (R_A^2 + R_B^2)}{d^8} \right. \\ \left. + \frac{64 (5 R_A^7 R_B^3 + 14 R_A^5 R_B^5 + 5 R_A^3 R_B^7)}{5d^{10}} \right) + \dots \tag{17}$$

For two identical spheres we can easily obtain the values of C_6^H, C_8^H, C_{10}^H from the simpler expression $E^H(R, d) = -\frac{\pi^2 \beta}{6} \left(\frac{32 R^6}{3d^6} + \frac{64 R^8}{d^8} + \frac{1536 R^{10}}{5d^{10}} \right) + \dots$.

3.4 Calculation of Binding Energy Using the Unmodified Hamaker Expression

Simpler than in (15), Hamaker's [41] expression can be used without modification as a long-range vdW additive correction to the DFT results. We have used

$$E_{\text{MGGA-MS2+H}}(d') = E^H(d') + E_{\text{MGGA-MS2}}(d) \\ = \left[-\frac{\pi^2 \beta}{6} \left\{ \frac{2 R_A R_B}{d'^2 - (R_A + R_B)^2} + \frac{2 R_A R_B}{d'^2 - (R_A - R_B)^2} \right. \right. \\ \left. \left. + \ln \left[\frac{d'^2 - (R_A + R_B)^2}{d'^2 - (R_A - R_B)^2} \right] \right\} \right] + E_{\text{MGGA-MS2}}(d). \tag{18}$$

Here β is calculated in the same way as is done for $E^H(R_A, R_B, d)$ as discussed in the above section. (See Appendix 1 for an explanation of $E^H(d)$.) In this version, no input vdW coefficient is needed.

4 Results and Discussion

We believe MGGA-MS2 gives better result than other semilocal GGA and *meta*-GGA functionals (PBE,TPSS) in our calculation because it uses "α" [18–20] which can recognize and describe the intermediate-range vdW interaction [20].

4.1 Ar–Ar Dimer

In Fig. 2 for Ar_2, binding energy curves are calculated using MGGA-MS2, MGGA-MS2 + vdW[d], MGGA-MS2 + vdW[d'], MGGA-MS2 + H[d], MGGA-MS2 + H [d'], vdW-DF2, and PBE-D2, and are compared with the experimental results [47]. The binding energy (ΔE in kcal/mol) and the equilibrium distance (R_e in Å) for different methods are tabulated in Table 3 along with the experimental results. Figure 2a shows that the MGGA-MS2 + vdW[d'] is in very good agreement with the experimental curve, whereas MGGA-MS2 binds slightly less than the experimental curve. In this figure the MGGA-MS2 + vdW[d] curve is calculated by adding the van der Waals correction part to the MGGA-MS2 result, but without using the cut-off distance d', and thus it clearly depicts the divergence near $d = 2R$. The interesting thing about this graph is that MGGA-MS2 gives a comparatively good intermediate-range part of the binding energy curve as expected [19, 20], slightly overestimating the equilibrium bond length ~3.75 Å compared to the experimental one at 3.76 Å. Figure 2a also shows that at larger atomic separation MGGA-MS2 significantly underbinds the experimental binding energy curve. Figure 2b shows
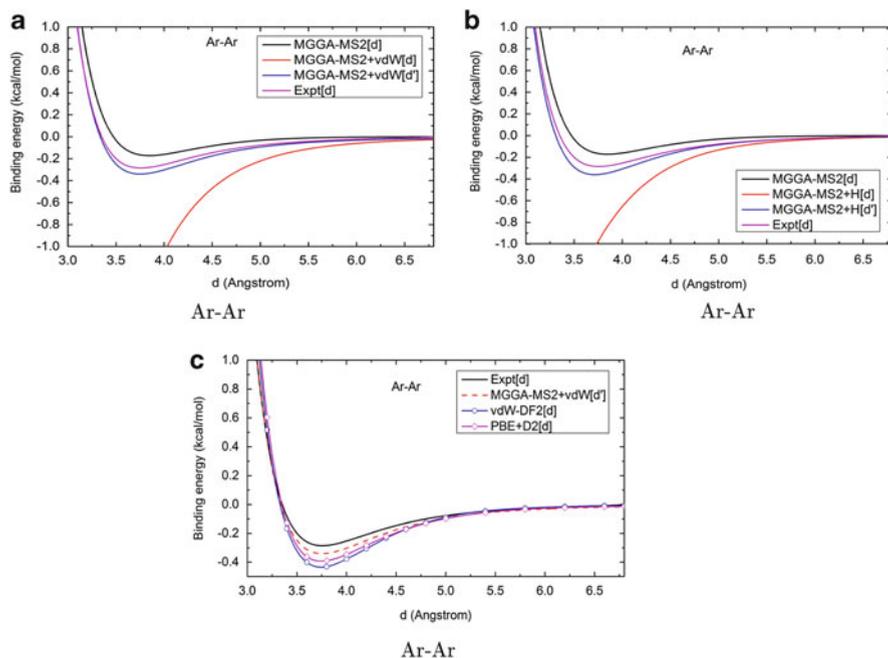
Fig. 2 Binding energy curves for the Ar–Ar dimer calculated from the vdW method combined with MGGA-MS2 using the system-averaged $a = 2.09$. (**a**) Binding energy curves for MGGA-MS2, MGGA-MS2 + vdW[d], MGGA-MS2 + vdW[d'], and experiment. (**b**) Binding energy curves for MGGA-MS2, MGGA-MS2 + H[d], MGGA-MS2 + H[d'], and the experimental curve. (**c**) Comparison of the vdW-DF2 [46] and PBE-D2 [27] curves with the experimental one

Table 3 Binding energy (ΔE in kcal/mol) and equilibrium bond length (R_e in Å) for the Ar–Ar dimer

Quantity	MGGA-MS2	MGGA-MS2 + vdW(d')	MGGA-MS2 + H(d')	PBE-D2	vdW-DF2	Expt.
ΔE	0.17206	0.34025	0.36057	0.38889	0.43207	0.28500
R_e	3.85	3.75	3.72	3.80	3.80	3.76
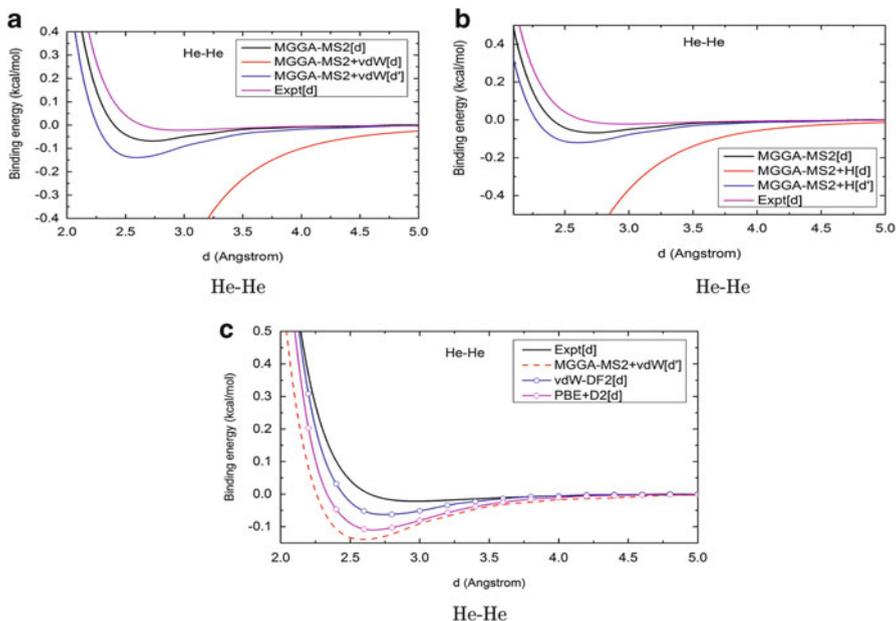
Fig. 3 Binding energy curves of the He–He dimer. Here we have also used the cut-off distance d' for long-range correction with the system-averaged $a = 2.09$. (**a**, **b**) Binding energy curves for MGGA-MS2, MGGA-MS2 + vdW[d], MGGA-MS2 + vdW[d'], MGGA-MS2 + H[d], and MGGA-MS2 + H[d']. (**c**) Comparison of the curves for vdW-DF2 [46] and PBE-D2 [27] with the experimental curve

that when the unmodified Hamaker (E^H) expression is used, it also gives a very good long-range part of the interaction potential, although MGGA-MS2 + H[d'] slightly overbinds the experimental curve. The divergence in the additive correction part (see MGGA-MS2 + H[d] curve) can be seen as for the vdW correction part in Fig. 2a. We also calculated the binding energy curves of the Ar–Ar dimer with the two popular van der Waals corrected methods vdW-DF2 [46] and PBE-D2 [27]. The binding energy curves from these calculations along with the MGGA-MS2 + vdW[d'] and experimental results can be seen in Fig. 2c. Both vdW-DF2 and PBE-D2 overbind the experimental binding energy curve in the range 3.3 Å $\leq R_e \leq$ 5.4 Å. Figure 3c also shows that MGGA-MS2 + vdW[d'], PBE-D2, and vdW-DF2 almost overlap with the experimental curve beyond 5.10 Å.

Table 4 Binding energy (ΔE in kcal/mol) and equilibrium bond length (R_e in Å) for the He–He dimer

Quantity	MGGA-MS2	MGGA-MS2 + vdW(d')	MGGA-MS2 + H(d')	PBE-D2	vdW-DF2	Expt.
ΔE	0.06849	0.13913	0.12038	0.10742	0.06214	0.02201
R_e	2.73	2.59	2.61	2.60	2.80	2.97

4.2   He–He Dimer

Figure 3 shows the binding energy curves for He$_2$ from MGGA-MS2, MGGA-MS2 + vdW[d],   MGGA-MS2 + vdW[d'],   MGGA-MS2 + H[d],   MGGA-MS2 + H[d'], vdW-DF2, and PBE-D2 calculations, along with the experimental results [47]. As predicted by Ruzsinszky et al. [24], nonempirical GGAs and *meta*-GGAs tend to overbind van der Waals-bound diatomics that have valence "s" electrons, such as He$_2$. Figure 3a shows that MGGA-MS2 and MGGA-MS2 + vdW[d'] overbind the experimental curve. When we plot MGGA-MS2 + vdW[d] we observe a divergence similar to the one for the Ar dimer because, in this case, the cut-off d' has not been used to remove the singularity. This graph also shows very good long-range behavior of MGGA-MS2 + vdW [d']. Figure 3b shows an almost similar picture where MGGA-MS2 + H [d'] also overbinds the experimental curve. In this case, a divergence in the Hamaker (E^H) expression can be seen. From Table 4 we note that the strong attractive nature of MGGA-MS2 yields a minimum at 2.73, 2.59, and 2.61 Å for MGGA + MS2, MGGA + MS2 + vdW[d'], and MGGA-MS2 + H[d'], respectively, which is quite different from the experimental one at 2.97 Å. From Fig. 3c we can see that two other popular methods, PBE-D2 [27] and vdW-DF2 [46], overbind the experimental curve in the same way as MGGA-MS2 + vdW(d'), but all these three curves almost overlap with the experimental curve in the very long-range part beyond 4.00 Å, a significant success for the method.

4.3   Xe–Xe Dimer

In the Xe–Xe dimer, MGGA-MS2, MGGA-MS2 + vdW[d'], and MGGA-MS2 + H [d'] underbind the experimental curve, which can be seen in Fig. 4a, b. These two graphs also show similar divergences for MGGA-MS2 + vdW[d] and MGGA-MS2 + H[d] because of the singularity near $d = 2R$ in both the vdW correction part and in the Hamaker expression. Figure 4c compares PBE-D2 [27], vdW-DF2 [46], and MGGA-MS2 + vdW[d'] with the experimental curve. From these three figures, and from Table 5, it can be said that, where PBE-D2 and vdW-DF2 overestimate the binding energy, MGGA-MS2 + vdW[d'] and MGGA-MS2 + H[d'] underestimate the same, but all these four methods give very different minima than the experimental one.
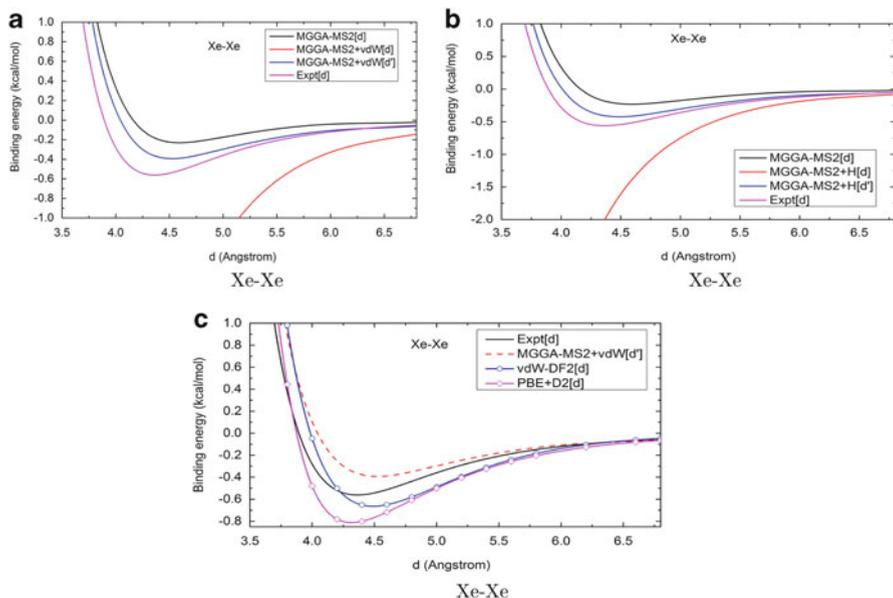
Fig. 4 (**a**) Binding energy curves for MGGA-MS2, MGGA-MS2 + vdW[d], and MGGA-MS2 + vdW[d']. (**b**) Binding energy curves for MGGA-MS2, MGGA-MS2 + H[d], and MGGA-MS2 + H[d']. (**c**) Binding energy curves using vdW-DF2 [46] and PBE-D2 [27] plotted with the experimental one

Table 5 Binding energy (ΔE in kcal/mol) and equilibrium bond length (R_e in Å) for the Xe–Xe dimer

Quantity	MGGA-MS2	MGGA-MS2 + vdW(d')	MGGA-MS2 + H(d')	PBE-D2	vdW-DF2	Expt.
ΔE	0.23100	0.39302	0.42232	0.80012	0.65163	0.56057
R_e	4.59	4.53	4.54	4.40	4.40	4.35

4.4 Kr–Kr Dimer

Figure 5a–c shows the binding energy curves for the Kr–Kr dimer for MGGA-MS2, MGGA-MS2 + vdW[d], MGGA-MS2 + vdW[d'], MGGA-MS2 + H[d], MGGA-MS2 + H[d'], vdW-DF2, and PBE-D2 approaches. These curves show that both MGGA-MS2 + vdW[d'] and MGGA-MS2 + H[d'] give a very satisfactory long-range part of the van der Waals interaction. It should be noted that these two curves cross the experimental curve at R(Kr–Kr) ~4.1 Å and at ~3.77 Å. One can readily note the divergence of MGGA-MS2 + H[d] at small atomic separation because of the obvious singularity in the expression of E^H. Table 6 gives the binding energy
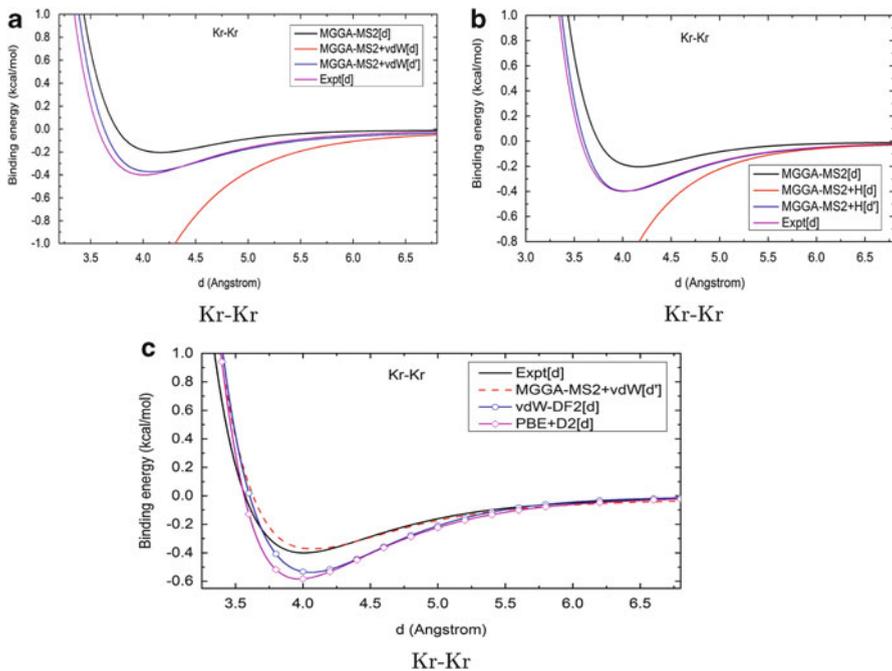
Fig. 5 (**a**) Binding energy curves for MGGA-MS2, MGGA-MS2 + vdW[d], and MGGA-MS2 + vdW[d']. (**b**) Binding energy curves for MGGA-MS2, MGGA-MS2 + H[d], and MGGA-MS2 + H[d']. (**c**) Binding energy curves using vdW-DF2 [46] and PBE-D2 [27] plotted with the experimental one. The vdW corrected curves are calculated using the cut-off distance d' and system-averaged $a = 2.09$

Table 6 Binding energy (ΔE in kcal/mol) and equilibrium bond length (R_e in Å) for the Kr–Kr dimer

Quantity	MGGA-MS2	MGGA-MS2 + vdW(d')	MGGA-MS2 + H(d')	PBE-D2	vdW-DF2	Expt.
ΔE	0.20379	0.37102	0.39750	0.53832	0.53242	0.40005
R_e	4.17	4.11	4.03	4.00	4.00	4.01

(ΔE in kcal/mol) and the equilibrium distance (R_e in Å) for different methods. We notice that MGGA-MS2 + H[d'] gives very good equilibrium bond length when compared to the experimental result. Figure 5c confirms that another two methods, PBE-D2 [27] and vdW-DF2 [46], significantly overbind the experimental curve. We can see the same trend in MGGA-MS2 + vdW[d'] along with PBE-D2 and vdW-DF2 in the very long-range part, where they tend to overlap with the experimental result.

4.5   Ne–Ne Dimer

In the Ne–Ne dimer, MGGA-MS2, MGGA-MS2 + vdW [d'], and MGGA-MS2 + H [d'] overbind the experimental curve. MGGA-MS2 + H[d] and MGGA-MS2 + vdW [d] show the divergence at small atomic separation. However, Fig. 6a, b shows the similar kind of long-range correction by both MGGA-MS2 + vdW[d'] and MGGA-MS2 + H[d']. We plot the PBE-D2 and vdW-DF2 result with the experimental and MGGA-MS2 + vdW[d'] results in Fig. 6c. We conclude that, for the Ne dimer, semilocal functionals normally overbind the experimental result. From Fig. 6c we find that the long-range part of the MGGA-MS2 + vdW[d'] and vdW-DF2 curves almost overlap with the experimental curve in the range 3.9 Å $\leq R_e \leq$ 5.0 Å. Table 7 shows numerical values.
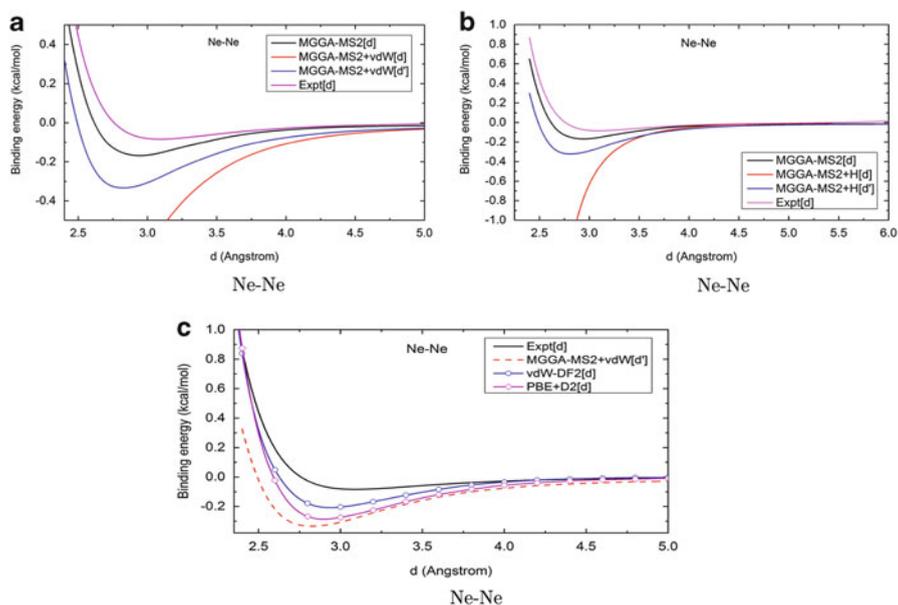
Fig. 6 Binding energy curves for the Ne–Ne dimer: (**a**) for MGGA-MS2, MGGA-MS2 + vdW[d], and MGGA-MS2 + vdW[d']; (**b**) for MGGA-MS2, MGGA-MS2 + H[d], and MGGA-MS2 + H[d']. (**c**) Comparison of the calculated binding energy curves using vdW-DF2 [46] and PBE-D2 [27] with the experimental curve

Table 7 Binding energy (ΔE in kcal/mol) and equilibrium bond length (R_e in Å) for the Ne–Ne dimer

Quantity	MGGA-MS2	MGGA-MS2 + vdW(d')	MGGA-MS2 + H(d')	PBE-D2	vdW-DF2	Expt.
ΔE	0.16811	0.33323	0.32208	0.27369	0.20395	0.08401
R_e	2.94	2.83	2.81	3.00	3.00	3.09

4.6 Ar–Kr Dimer

MGGA-MS2 underbinds the experimental curve [48] in the Ar–Kr dimer, as can be seen in Fig. 7a, b. This tendency is removed and we get very satisfactory binding energy curves when the cut-off distance d' is introduced in the MGGA-MS2 + vdW [d'] and MGGA-MS2 + H[d'] methods. This removes the singularity as expected and gives significant improvement in the long-range part of the van der Waals interaction. The strong divergence in van der Waals interaction series and in Hamaker's expression can be seen in MGGA-MS2 + vdW[d] and in MGGA-MS2 + H[d] in Fig. 7a, b. PBE-D2 [27] and vdW-DF2 [46] results are not so satisfactory compared to the experimental result. Table 8 shows the binding energy (ΔE in kcal/mol) and the equilibrium distance (R_e in Å) for different methods.
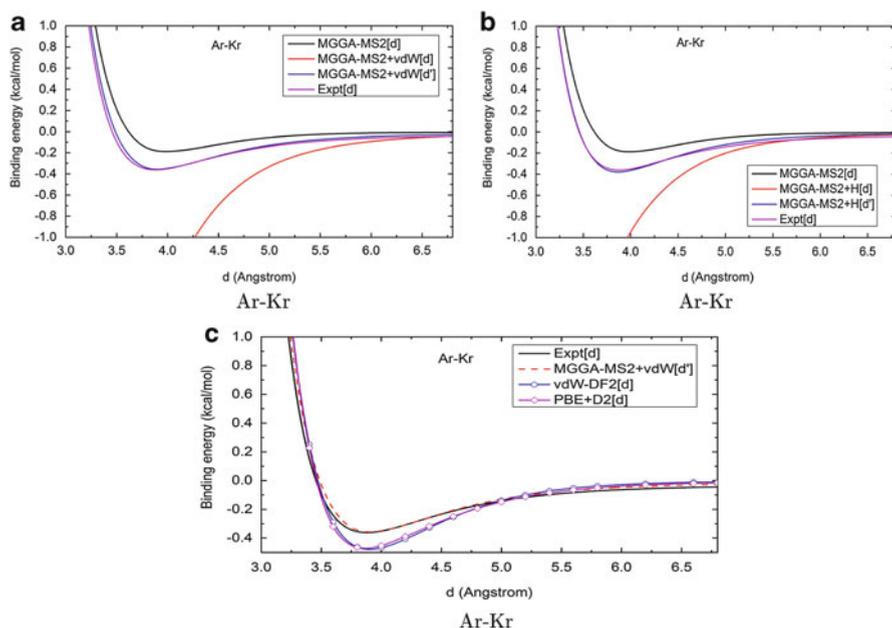
Fig. 7 Binding energy curves of the Ar–Kr dimer calculated: (**a**) using MGGA-MS2, MGGA-MS2 + vdW[d], and MGGA-MS2 + vdW[d']; (**b**) using MGGA-MS2, MGGA-MS2 + H[d], MGGA-MS2 + H[d'], and the experimental result. (**c**) Comparison of vdW-DF2 [46] and PBE-D2 [27] with experiment. The vdW corrected binding energy curves are calculated using the cut-off distance d' and system-averaged $a = 2.09$

Table 8 Binding energy (ΔE in kcal/mol) and equilibrium bond length (R_e in Å) for the Ar–Kr dimer

Quantity	MGGA-MS2	MGGA-MS2 + vdW(d')	MGGA-MS2 + H(d')	PBE-D2	vdW-DF2	Expt.
ΔE	0.18772	0.35712	0.38053	0.46469	0.46481	0.36123
R_e	3.98	3.89	3.88	3.80	4.00	3.88

4.7 Ar–Xe Dimer

We plot the binding energy curves of the Ar–Xe dimer in Fig. 8a, b. These figures show outstanding performance of the method in the long-range part of the energy when either of the additive corrections $E_{vdW}(d')$ or $E^H(d')$ is used. Table 9 gives a qualitative picture of different methods for the estimation of equilibrium bond length and binding energy. It can be inferred from Table 9 that both MGGA-MS2 + vdW [d'] and MGGA-MS2 + H[d'] produce almost correct binding energy but slightly overestimate the equilibrium bond length.
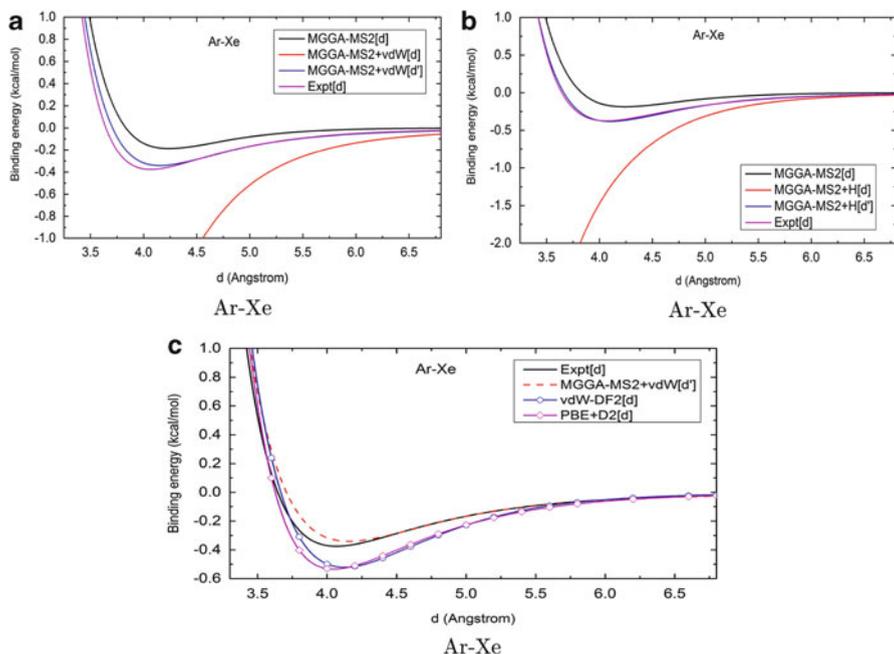
Fig. 8 Binding energy curves of the Ar–Xe dimer calculated from the vdW method combined with MGGA-MS2 using the system-averaged a. (**a**) Binding energy curves calculated using MGGA-MS2, MGGA-MS2 + vdW[d], and MGGA-MS2 + vdW[d'], and the experimental one. The vdW-corrected binding energy curve is calculated using the cut-off distance d' and system-averaged $a = 2.09$. (**b**) Binding energy curves for MGGA-MS2, MGGA-MS2 + H[d], and MGGA-MS2 + H[d'], and the experimental results. (**c**) Binding energy curves from other vdW-corrected methods

Table 9 Binding energy (ΔE in kcal/mol) and equilibrium bond length (R_e in Å) for the Ar–Xe dimer

Quantity	MGGA-MS2	MGGA-MS2 + vdW(d')	MGGA-MS2 + H(d')	PBE-D2	vdW-DF2	Expt.
ΔE	0.18677	0.34032	0.38191	0.53029	0.51532	0.37505
R_e	4.24	4.10	4.10	4.00	4.20	4.07

4.8 Kr–Xe Dimer

As in the Ar–Kr dimer, in the Kr–Xe dimer MGGA-MS2 underbinds the experimental curve. Figure 9a, b shows that introduction of the cut-off distance d' not only removes the singularity but also improves the underbinding of MGGA-MS2 in the long-range part of the van der Waals interaction energy, although it remarkably overestimates the equilibrium bond length. The binding energy estimated by MGGA-MS2 + H [d'] is in very good agreement with the experimental result. The PBE-D2, vdW-DF2, MGGA-MS2 + vdW[d'], and experimental curves are shown in Fig. 9c. PBE-D2 and vdW-DF2 seem to be too attractive in the short-range part and overbind the experimental curve, although the equilibrium bond lengths from these two curves are in very good agreement with experiment. Table 10 shows numerical values.
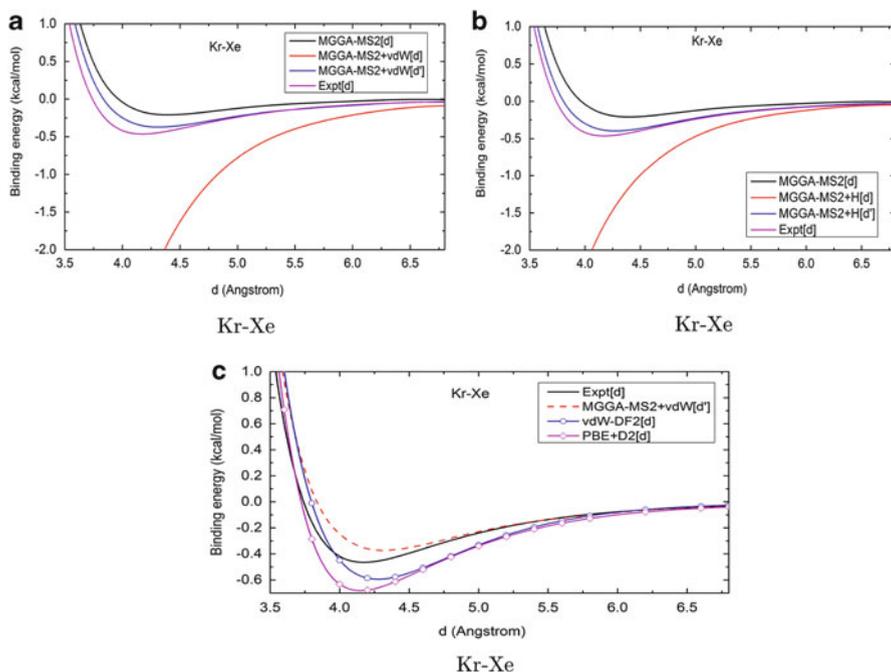
Fig. 9 Binding energy curves of the Kr–Xe dimer calculated from the vdW method combined with MGGA-MS2 using the system-averaged $a = 2.09$. (**a**) Binding energy curves for MGGA-MS2, MGGA-MS2 + vdW[d], and MGGA-MS2 + vdW[d'], and the experimental one. (**b**) Binding energy curves for MGGA-MS2, MGGA-MS2 + H[d], and MGGA-MS2 + H[d'], and the experimental results. (**c**) Comparison of vdW-DF2 [46] and PBE-D2 [27] with experiment

Table 10 Binding energy (ΔE in kcal/mol) and equilibrium bond length (R_e in Å) for the Kr–Xe dimer

Quantity	MGGA-MS2	MGGA-MS2 + vdW(d')	MGGA-MS2 + H(d')	PBE-D2	vdW-DF2	Expt.
ΔE	0.20900	0.37242	0.39787	0.67692	0.58528	0.46422
R_e	4.39	4.31	4.27	4.20	4.20	4.18
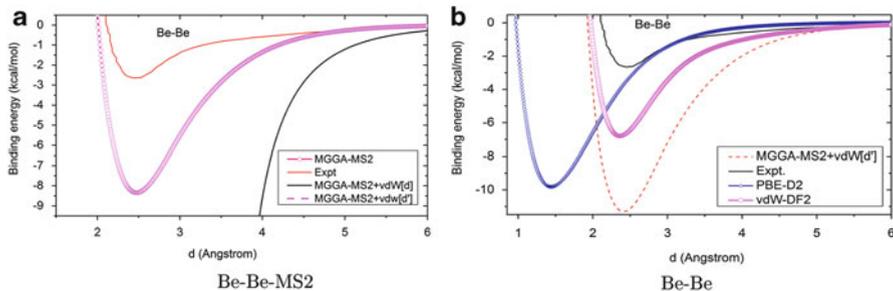
Fig. 10 Binding energy curves for the Be–Be dimer calculated (**a**) from *meta*-GGA-MS2 and (**b**) from other vdW-corrected methods

4.9   Be–Be Dimer

Be_2 is chosen because it is a van der Waals-bound diatomic from the alkaline earth group. The characteristic difference of Be_2 from the rare gas dimers is that it shows much more density overlap. Figure 10a gives us a qualitative picture of how the strong divergence at $d = 2R$ in the $E^H(d)$ part of the van der Waals interactions energy expression of (15) is successfully removed upon introduction of the cut-off distance d'. Figure 10b shows that MGGA-MS2 + vdW [d'] gives a satisfactory long-range correction compared to PBE-D2. In the same figure the similar performance of vdW-DF2 can be seen. The common tendency of overbinding the experimental result [49] by semilocal functionals MGGA-MS2 and PBE [24] can be seen in Fig. 10b. From this result we conclude that more accurate correction is needed for semilocal functionals for He_2, Ne_2, and Be_2. Moreover, Fig. 10b shows that vdW-DF2 correctly estimates the equilibrium bond length ~2:5 Å, where MGGA-MS2 + vdW[d'] fails to do so. It overestimates the bond length at ~2.7 Å. The experimental equilibrium bond length is 2.45 Å. Careful observation of Fig. 10b reveals that the too-attractive nature of PBE yields a deep minimum at very short distance ~1.5 Å for the PBE-D2 curve.

4.10   Comparison Between Hamaker and Geometric Series for Two Identical Solid Spheres

An interesting feature of the Hamaker expression [41] and the geometric expression [38] (see (25) in Appendix 1) is that both have divergences at two different values of d, one at $d = 2R$ and the other at $d = 0$. To investigate further the divergence of these two expressions, we have plotted $c_\infty \left\{ \left(1 - \left(\frac{2R}{d} \right)^2 \right) \right)^{-1} - \sum_{k=0}^{2} \left(\frac{2R}{d} \right)^{2k} \right\}$ and $\left(\frac{c_\infty}{c_\infty^H} \right) E^H(R_A = R_B = R, d)$. These two quantities have the same singularity at $d = 2R$ but they are rather different in the range of typical vdW energies, which can be seen in Fig. 11. This could explain why the Hamaker expression works better in the fits.

Fig. 11 Divergence of Hamaker's [41] expression and the geometric expression of Perdew et al. [38] for Ar–Ar dimer
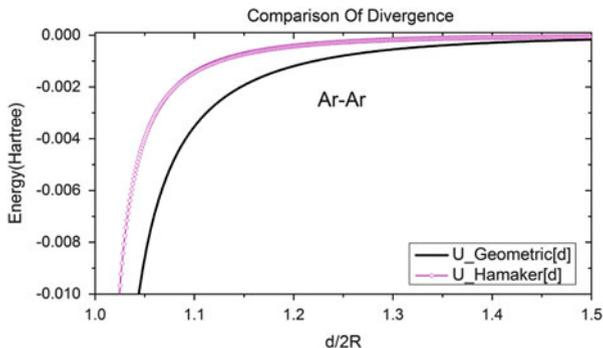
5 Conclusions

In summary, our work is a reasonable and physical way to remove the nonzero d singularity in the summed-up van der Waals interaction series. We also conclude that, although the fitting parameter "a" is system-dependent and empirical in nature, averaging it and using $R = \max(R^{hbl}, 1.37R^{po1})$ as an input to our calculation gives our formulas some predictive value. In this work we have presented a simplified version with only one fitting parameter a, replacing the earlier model [38] with two parameters (g, h), to get the long-range van der Waals correction to a density-functional binding energy curve for objects with spherical densities. We have reached similar or better accuracy when compared with the PBE-D2 [27] and vdW-DF2 [46] correction schemes.

An interesting outcome of our work is that the complicated (15), as proposed in Perdew et al. [38], can be replaced without loss of accuracy by the simpler (18). This means in particular that no input vdW coefficient is needed.

One extension of this work could be to use it to obtain a semi-local density functional with an embedded long-range vdW correction using this summed-up series method. The positive outcome of this method motivates us to use it for other strongly dispersion-driven systems such as layered-materials. Furthermore, MGGA-MS2 often provides a useful description of intermediate-range vdW interaction. It underestimates this in most rare gas dimers, but overestimates it in He_2, Ne_2, and Be_2. Appreciable performance by MGGA-MS2 [19] in predicting stacking energies between nucleobases of DNA and RNA confirms that improved density functionals can give a better description of different chemical and physical properties. It remains to be seen whether further improvements in *meta*-GGAs yield a more consistent description of intermediate-range vdW interactions.

Appendix 1 Summed-Up Series Expression

The Casimir–Polder [50, 51] formula for the van der Waals coefficients between two objects A and B to the second-order in electron–electron interaction is

$$C_{2k}^{AB} = \frac{(2k-2)!}{2\pi} \sum_{l_1=1}^{k-2} \frac{1}{(2l_1)!(2l_2)!} \int_0^\infty du\, \alpha_{l_1}^A(iu)\alpha_{l_2}^B(iu), \tag{19}$$

where $l_2 = k - l_1 - 1$ and $\alpha_{l_1}^A \to 2^{l_1}$ pole dynamic polarizability of A at imaginary frequency $\omega = iu$. It should be noted that $l = 1$, $l = 2$, $l = 3$ are for dipole, quadrupole, and octupole interactions, respectively.

The dynamic multipole polarizabilities for a classical conducting spherical shell can be found from the following expressions:

$$\alpha_l(iu) = R^{2l+1} \frac{\omega_l^2}{\omega_l^2 + u^2} \frac{1 - \theta_l}{1 - \beta_l \theta_l}, \tag{20}$$

where

$$\beta_l = \frac{\omega_l^2 \widetilde{\omega}_l^2}{(\omega_l^2 + u^2)(\widetilde{\omega}_l^2 + u^2)} \tag{21}$$

and

$$\theta_l = \left(\frac{R-t}{R}\right)^{2l+1} = (1 - t/R)^{2l+1} \tag{22}$$

from the work of Lucas et al. [52]. Here $\omega_l = \omega_p \sqrt{l/(2l+1)}$ and $\widetilde{\omega}_l = \omega_p \sqrt{(l+1)/(2l+1)}$. The plasma frequency of the system is $\omega_p = \sqrt{4\pi\rho}$ with $\rho = \frac{N}{\left[\frac{4}{3}\pi\{R^3 - (R-t)^3\}\right]}$ for the spherical shell (with radius R and thickness t) and $\rho = \frac{N}{\left(\frac{4}{3}\pi R^3\right)}$ for the sphere (with radius R). N is the total number of valence electrons, equal to 2 for He and 8 for other rare gas atoms.

In Perdew et al. [37] it is shown that, for a classical conducting spherical shell of radius R, thickness t, and uniform density ρ, the above integration at (18) can be performed to get all the higher order vdW coefficients. For two identical spheres, i.e., when $A = B$, one can get

$$C_{2k}^{AA} = \omega_p (2R)^{2k} \frac{1}{2^{2k}} \frac{(2k-2)!}{4} \sum_{l=1}^{k-2} \frac{1}{(2l)!(2k-2l-1)!}$$
$$\times \frac{1}{\sqrt{(2l+1)/l} + \sqrt{(2k-2l-1)/(k-l-1)}}. \tag{23}$$

Then the van der Waals interaction of (2) can be written as

$$E(d) = -\sqrt{4\pi\rho} \sum_{k=3}^{\infty} c_k(t/R) z^k, \qquad (24)$$

where $c_k(t/R)$ is related to C_{2k} by (4) and $z = \left(\frac{2R}{d}\right)^2$.

Now, by the introduction of the geometric series of $\sum_{k=1}^{\infty} z^k = (1-z)^{-1}$ for $0 \le z < 1$ and approximating $c_k \to c_\infty$ for $k > 5$, we find

$$E^{\text{geo}}(d) = -\sqrt{4\pi\rho} \left[c_3\left(\frac{t}{R}\right) z^3 + c_4\left(\frac{t}{R}\right) z^4 + c_5\left(\frac{t}{R}\right) z^5 + c_\infty \left\{ (1-z)^{-1} - \sum_{k=0}^{5} z^k \right\} \right].$$

$$(25)$$

This expression interpolates between the very large d and $d \to 2R$ limits. The above expression for $E^{\text{geo}}(d)$ has an unphysical divergence at $z = 1$ or $d = 2R$ where the two spheres touch each other. This divergence appears because we sum up all the terms. However, in reality there is no divergence in (2) because it is an asymptotic expansion for large value of d.

This is true because at large d the exponential density overlap between the two real quantum-mechanical objects may be neglected. This divergence in the expression of $E^{\text{geo}}(d)$ can be removed by replacing z by z' where $z' = (2R/d')^2$ with a proper choice of d'. The expression for $E^{\text{geo}}(d)$ is true for the interaction between identical spheres but it can be generalized to non-identical spheres $2R \to R_A + R_B$, which leads to an equation such as (14) for the expression of $E_{\text{vdW}}(d')$.

In the pair interaction picture, Hamaker's [41] expression of the van der Waals interaction between two solid spheres of uniform density ρ is

$$E(d) = -\beta \int_A d^3r \int_B d^3r' \frac{1}{|r - r'|^6}, \qquad (26)$$

where $\beta = c_3(1)\sqrt{4\pi\rho}\left(\frac{3}{4\pi}\right)^2 2^6 = 0.006766\sqrt{4\pi\rho}\left(\frac{3}{4\pi}\right)^2 2^6$ can be evaluated using the value of $c_3(1)$ from Table 1.

Appendix 2 Binding Energy Curves from Geometric Series

The summed-up van der Waals series expression of (4) can also be used to obtain the binding energy curves for the rare-gas dimers if we use our short-range cut-off idea. Reduced van der Waals coefficients $c_3(t/R)$, $c_4(t/R)$, $c_5(t/R)$ and $c_\infty(t/R)$ are taken from Table 1 for $t/R = 1$, e.g., for solid spheres. For identical solid-spheres the electron density is $\rho = N/\left(4\pi R^3/3\right)$ for a sphere with radius R and number of total valence electrons N (N is 2 for He and 8 for the other rare-gas atoms). The electron density for non-identical spheres can be evaluated using $2\sqrt{\rho_A}\sqrt{\rho_B}/\left(\sqrt{\rho_A} + \sqrt{\rho_B}\right)$.

We could not optimize the fitting parameter for every dimer. We have used $a = 4.09$, the average of the optimum values for Ar–Ar and Kr–Kr. Figure 12 shows the results.
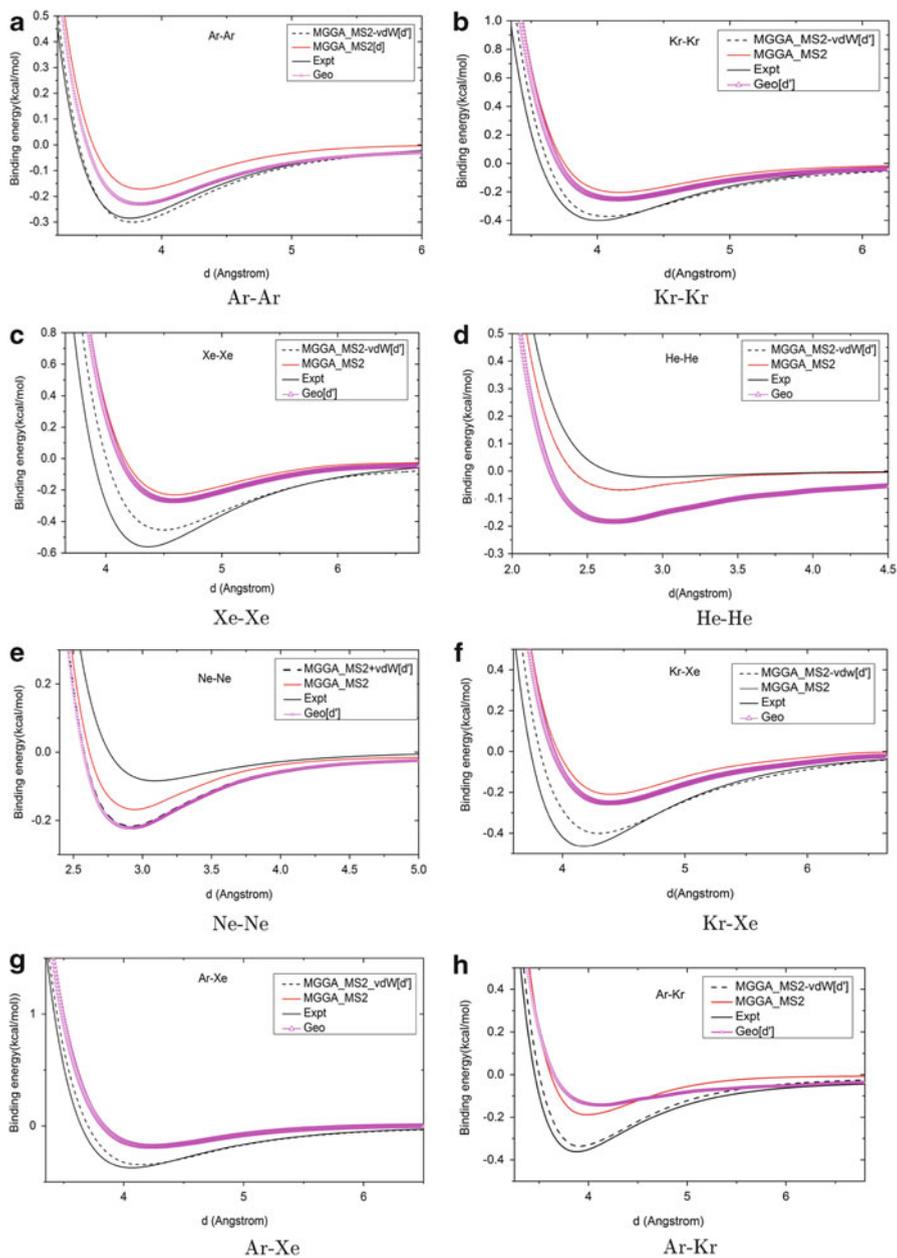
Fig. 12 Binding energy curves for different dimers using the geometric-series expression of (25) $a = 4.09$

References

1. Kohn W, Sham LJ (1965) Self-consistent equations including exchange and correlation effects. Phys Rev 140:A1133–A1138
2. Perdew JP, Kurth S (2003) A primer in density functional theory, Lecture notes in physics. Springer, Berlin
3. Perdew JP, Wang Y (1992) Accurate and simple analytic representation of the electron-gas correlation energy. Phys Rev B 45:13244–13249
4. Sun J, Perdew JP, Seidl M (2010) Correlation energy of the uniform electron gas from an interpolation between high- and low-density limits. Phys Rev B 81(8):085123
5. Perdew JP, Burke K, Ernzerhof M (1996) Generalized gradient approximation made simple. Phys Rev Lett 77:3865–3868
6. Becke AD (1993) Density functional thermochemistry, III. The role of exact exchange. J Chem Phys 98(7):5648–5652
7. Heyd J, Scuseria GE, Ernzerhof M (2003) Hybrid functionals based on a screened Coulomb potential. J Chem Phys 118(18):8207–8215
8. Paier J, Marsman M, Hummer K, Kresse G, Gerber IC, Ángyán JG (2006) Screened hybrid density functionals applied to solids. J Chem Phys 124(15):154709
9. Burke K (2012) Perspective on density functional theory. J Chem Phys 136(139):150901
10. Perdew JP, Schmidt K (2001) Jacob's ladder of density functional approximations for the exchange-correlation energy. AIP Conf Proc 577(1):1–20
11. Tao J, Perdew JP, Staroverov VN, Scuseria GE (2003) Climbing the density functional ladder: nonempirical meta-generalized gradient approximation designed for molecules and solids. Phys Rev Lett 91:146401
12. Perdew JP, Ruzsinszky A, Csonka GI, Vydrov OA, Scuseria GE, Constantin LA, Zhou X, Burke K (2008) Restoring the density-gradient expansion for exchange in solids and surfaces. Phys Rev Lett 100:136406
13. Perdew JP, Ruzsinszky A, Csonka GI, Constantin LA, Sun J (2009) Workhorse semilocal density functional for condensed matter physics and quantum chemistry. Phys Rev Lett 103:026403
14. Staroverov VN, Scuseria GE, Tao J, Perdew JP (2003) Comparative assessment of a new nonempirical density functional: molecules and hydrogen-bonded complexes. J Chem Phys 119:12129
15. Perdew JP, Ruzsinszky A, Tao J, Csonka GI, Scuseria GE (2007) One-parameter optimization of a nonempirical meta-generalized-gradient-approximation for the exchange-correlation energy. Phys Rev A 76(4):042506
16. Tao J, Perdew JP, Ruzsinszky A, Scuseria GE, Csonka GI, Staroverov VN (2007) Meta-generalized gradient approximation: non-empirical construction and performance of a density functional. Philos Mag 87(7):1071–1084
17. Constantin LA, Perdew JP, Tao J (2006) Meta-generalized gradient approximation for the exchange-correlation hole with an application to the jellium surface energy. Phys Rev B 73 (20):205104
18. Sun J, Xiao B, Ruzsinszky A (2012) Communication: effect of the orbital-overlap dependence in the meta generalized gradient approximation. J Chem Phys 137(5):051101
19. Sun J, Xiao B, Fang Y, Haunschild R, Hao P, Ruzsinszky A, Csonka GI, Scuseria GE, Perdew JP (2013) Density functionals that recognize covalent, metallic, and weak bonds. Phys Rev Lett 111(10):106401
20. Sun J, Haunschild R, Xiao B, Bulik IW, Scuseria GE, Perdew JP (2013) Semilocal and hybrid *meta*-generalized gradient approximations based on the understanding of the kinetic-energy-density dependence. J Chem Phys 138(4):044113
21. Zhao Y, Truhlar DG (2006) Comparative DFT study of van der Waals complexes: rare-gas dimers, alkaline-earth dimers, zinc dimer, and zinc-rare-gas dimers. J Phys Chem A 110 (15):5121–5129

22. Tran F, Hutter J (2013) Nonlocal van der Waals functionals: the case of rare-gas dimers and solids. J Chem Phys 138(20):204103
23. Tao J, Perdew JP (2005) Test of a non-empirical density functional: short-range part of the van der Waals interaction in rare-gas dimers. J Chem Phys 122(11):114102
24. Ruzsinszky A, Perdew JP, Csonka GI (2005) Binding energy curves from nonempirical density functionals II. van der Waals bonds in rare-gas and alkaline-earth diatomics. J Phys Chem A 109(48):11015–11102
25. Stone AJ (1996) The theory of intermolecular forces, vol 32, International series of monographs on chemistry. Oxford University Press, Oxford
26. Wu Q, Ayers PW, Yang W (2003) Density-functional theory calculations with correct long-range potentials. J Chem Phys 119:2978
27. Grimme S (2006) Semiempirical GGA-type density functional constructed with a long-range dispersion correction. J Comput Chem 27:1787
28. Sato T, Tsuneda T, Hirao K (2007) Long-range corrected density functional study on weakly bound systems: balanced descriptions of various types of molecular interactions. J Chem Phys 126:234114/1
29. Vydrov OA, Scuseria GE (2006) Assessment of a long-range corrected hybrid functional. J Chem Phys 125:234109/1
30. Grimme S, Ehrlich S, Goerigk L (2011) Effect of the damping function in dispersion corrected density functional theory. J Comput Chem 32(7):1456–1465
31. Johnson ER, Becke AD (2005) A post-Hartree–Fock model of intermolecular interactions. J Chem Phys 123(2):024101
32. Tkatchenko A, Scheffler M (2009) Accurate molecular van der Waals interactions from ground-state electron density and free-atom reference data. Phys Rev Lett 102(7):073005
33. Vydrov OA, Van Voorhis T (2010) Dispersion interactions from a local polarizability model. Phys Rev A 81(6):062708
34. Klimeš J, Michaelides A (2012) Perspective: advances and challenges in treating van der Waals dispersion forces in density functional theory. J Chem Phys 137(12):120901
35. Tao J, Perdew JP, Ruzsinszky A (2012) Accurate van der Waals coefficients from density functional theory. Proc Natl Acad Sci 109(1):18–21
36. Tao J, Perdew JP, Ruzsinszky A (2013) Long-range van der Waals interaction. Int J Modern Phys B 27(18):30011
37. Perdew JP, Tao J, Hao P, Ruzsinszky A, Csonka GI, Pitarke JM (2012) Spherical-shell model for the van der Waals coefficients between fullerenes and/or nearly spherical nanoclusters. J Phys Condens Matter 24(42):424207
38. Perdew JP, Ruzsinszky A, Sun J, Glindmeyer S, Csonka GI (2012) van der Waals interaction as a summable asymptotic series. Phys Rev A 86(6):062714
39. Ruzsinszky A, Perdew JP, Tao J, Csonka GI, Pitarke JM (2012) van der Waals coefficients for nanostructures: fullerenes defy conventional wisdom. Phys Rev Lett 109(23):233203
40. Wu Q, Yang W (2002) Empirical correction to density functional theory for van der Waals interactions. J Chem Phys 116(2):515–524
41. Hamaker H (1937) The London-van der Waals attraction between spherical particles. Physica 4(10):1058–1072
42. Blöchl PE (1994) Projector augmented-wave method. Phys Rev B 50(24):17953
43. Kresse G, Hafner J (1993) *Ab initio* molecular dynamics for liquid metals. Phys Rev B 47:558–561
44. Kresse G, Hafner J (1994) *Ab initio* molecular-dynamics simulation of the liquid-metal–amorphous-semiconductor transition in germanium. Phys Rev B 49:14251–14269
45. Kresse G, Joubert D (1999) From ultrasoft pseudopotentials to the projector augmented-wave method. Phys Rev B 59:1758–1775
46. Lee K, Murray ED, Kong L, Lundqvist B, Langreth D (2010) Higher-accuracy van der Waals density functional. Phys Rev B 82:081101

47. Ogilvie JF, Wang FY (1992) Potential-energy functions of diatomic molecules of the noble
    gases I. Like nuclear species. J Mol Struct 273:277–290
48. Ogilvie JF, Wang FY (1993) Potential-energy functions of diatomic molecules of the noble
    gases: II. Unlike nuclear species. J Mol Struct 291(2):313–322
49. Schmidt MW, Ivanic J, Ruedenberg K (2010) Electronic structure analysis of the ground-state
    potential energy curve of Be2. J Phys Chem A 114(33):8687–8696
50. Casimir HBG, Polder D (1948) The influence of retardation on the London-van der Waals
    forces. Phys Rev 73:360–372
51. Patil SH, Tang KT (1997) Multipolar polarizabilities and two- and three-body dispersion
    coefficients for alkali isoelectronic sequences. J Chem Phys 106(6):2298–2305
52. Lucas AA, Henrard L, Lambin P (1994) Computation of the ultraviolet absorption and electron
    inelastic scattering cross section of multishell fullerenes. Phys Rev B 49:2888–2896